IOP Publishing New J. Phys. 27 (2025) 013003 https://doi.org/10.1088/1367-2630/ada574

New Journal of Physics
The open access journal at the forefront of physics

Deutsche Physikalische Gesellschaft DPG
IOP Institute of Physics

Published in partnership with: Deutsche Physikalische Gesellschaft and the Institute of Physics

OPEN ACCESS

RECEIVED
18 September 2024

REVISED
10 December 2024

ACCEPTED FOR PUBLICATION
3 January 2025

PUBLISHED
13 January 2025

PAPER

Superconductivity in Weyl semimetals with time reversal symmetry

Xuesong Bai[1], W LiMing[1] and Tao Zhou[1,2,*]

[1] Guangdong Basic Research Center of Excellence for Structure and Fundamental Interactions of Matter, Guangdong Provincial Key Laboratory of Quantum Engineering and Quantum Materials, School of Physics, South China Normal University, Guangzhou 510006, People's Republic of China
[2] Guangdong-Hong Kong Joint Laboratory of Quantum Matter, Frontier Research Institute for Physics, South China Normal University, Guangzhou 510006, People's Republic of China
* Author to whom any correspondence should be addressed.

E-mail: tzhou@scnu.edu.cn

Keywords: superconductivity, Weyl semimetal, time-reversal symmetry, surface state

Supplementary material for this article is available online

Abstract

This theoretical study delves into the superconducting traits of Weyl semimetals that possess time reversal symmetry, utilizing the Bogoliubov–de Gennes equations. Our meticulous self-consistent calculations have unveiled a dual superconducting gap at the surface. We have also contrasted these findings with the superconducting characteristics of models that exhibit broken time-reversal symmetry. Our analysis indicates that Weyl semimetals with unimpaired time-reversal symmetry not only sustain a complete energy gap but also display modified Fermi arc surface states, which are notably distinct from those in models with compromised time-reversal symmetry. This work bridges the gap between theoretical expectations and experimental observations, advancing our understanding of the superconducting properties of Weyl semimetals.

1. Introduction

Weyl semimetals are a captivating class of materials distinguished by their topologically nontrivial electronic properties [1]. Since their theoretical prediction and experimental validation in 2015 [2–5], these materials have garnered significant attention. Weyl semimetals are characterized by the presence of band crossing points, known as Weyl nodes, where low-energy excitations exhibit linear dispersion. The formation of these nodes is predicated on the violation of spatial inversion symmetry or time-reversal symmetry.

The theoretical framework for Weyl semimetals was established within condensed matter physics [6–9], diverging from high-energy physics. The identification of Weyl fermions in materials from the TaAs family has propelled these materials into the spotlight of condensed matter physics and materials science research. Weyl semimetals possess a range of intriguing properties, such as linear dispersion in electronic bands, gapless Weyl points, and Fermi arcs on their surfaces, making them ideal for studying novel electronic phases and quantum transport phenomena [10, 11].

Their potential applications span superconductivity, quantum phase transitions, and electronic topological effects [12, 13]. The superconducting state in Weyl systems is particularly notable, as it may enable the realization of Majorana bound states, which are of great interest for topological quantum computation. The possibility of exotic superconducting states, such as the Fulde–Ferrell–Larkin–Ovchinnikov (FFLO) state [14] or the odd-parity BCS state [15], has also been theorized within the Weyl framework.

Experimental observations of superconductivity in various Weyl semimetal materials have confirmed theoretical expectations [16–28]. The single-particle spectrum is a key tool for examining electronic structures and pairing states in unconventional superconductors, accessible through angle resolved photoemission spectroscopy (ARPES) [29] or scanning tunneling microscope (STM) experiments [30]. Theoretical understanding of the single-particle spectrum is derived from the computation of the single-particle Green's function.

Recent experimental work, such as the STM observation of a superconducting gap of approximately 20 meV in the Weyl semimetal t-$PtBi_2$, has provided valuable insights into the superconducting properties of these materials [31–34]. Notably, clear superconducting coherence peaks have been revealed at the gap edges in the STM spectra at the system surface. However, these experimental results present a significant divergence from previous theoretical calculations of the local density of states (LDOSs) at the surface of Weyl superconductors. Theoretically, for all pairing states, there were no obvious coherence peaks predicted at the system surface [35]. Particularly, due to the Fermi arc in the *s*-wave superconducting state, it was proposed that the density of states at zero energy would be large, with no gap features [36].

This discrepancy between experimental observations and theoretical predictions, particularly regarding the presence of coherence peaks and the nature of the superconducting gap, underscores the need for a reevaluation of theoretical models in light of actual material properties. Many theoretical models are predicated on the assumption of inversion symmetry and the breaking of time-reversal symmetry [14, 15, 35–40]. However, the t-$PtBi_2$ material demonstrates a distinct symmetry profile, preserving time-reversal symmetry while exhibiting broken inversion symmetry [41, 42]. This discrepancy calls for a more nuanced approach to modeling that reflects the true symmetry properties of the material under investigation.

In this paper, we delve into the single-particle spectra of superconducting Weyl semimetals, focusing on the impact of time-reversal symmetry. Through self-consistent calculations of the superconducting gap and an exploration of the LDOS spectra, we find that the surface spectrum is fully gapped, with the emergence of two coherence superconducting peaks, aligning with recent experimental results. These findings bridge the gap between theoretical expectations and experimental observations and contribute to a deeper understanding of the superconducting properties of Weyl semimetals.

The structure of this paper is as follows: section 2 introduces the model and the theoretical framework. Section 3 presents numerical calculations and discusses the results. Section 4 concludes with a summary of our findings.

2. Model and formalism

We commence our theoretical investigation with a model Hamiltonian that encompasses both the normal state and interaction terms:

$$H = H_0 + H_\Delta. \tag{1}$$

Here, H_0 denotes the normal state Hamiltonian, which represents the effective lattice model of a Weyl metal. It is expressed as:

$$H_0 = \sum_{\mathbf{k}} \Psi_{\mathbf{k}}^\dagger H_0(\mathbf{k}) \Psi_{\mathbf{k}}.$$

The matrix $H_0(\mathbf{k})$ is a 4×4 matrix, detailed as follows [43, 44]:

$$\begin{aligned} H_0(\mathbf{k}) = {} & \xi_k \sigma_0 \otimes \tau_0 + h\sigma_0 \otimes \tau_z + (t_z'' \sin k_z)\, \sigma_z \otimes \tau_z \\ & + t' \sin k_y (\sigma_z \otimes \tau_x) - t' \sin k_x (\sigma_0 \otimes \tau_y), \end{aligned} \tag{2}$$

where $\xi_k = -2t_1(\cos k_x + \cos k_y) - 2t_2 \cos k_z - \mu$, $h = t_z' \cos k_z + M(2 - \cos k_x - \cos k_y)$. σ_i and τ_i are the identity matrix ($i = 0$) and Pauli matrices ($i = 1, 2, 3$), respectively, operating in the spin and orbital channels. The wavevector $\Psi_{\mathbf{k}}$ is defined as: $\Psi_{\mathbf{k}} = (C_{1\mathbf{k}\uparrow}, C_{2\mathbf{k}\uparrow}, C_{1\mathbf{k}\downarrow}, C_{2\mathbf{k}\downarrow})^T$.

We define the time-reversal operator T and the inversion operator P as: $T = i\sigma_y \otimes \tau_0 K$ (K is the complex-conjugate operator) and $P = \sigma_0 \otimes \tau_z$. The normal state Hamiltonian H_0 exhibits time-reversal symmetry with $T^{-1} H_0(\mathbf{k}) T = H_0(-\mathbf{k})$.

When $t_z'' = 0$, the model also exhibits inversion symmetry: $P^{-1} H_0(\mathbf{k}) P = H_0(-\mathbf{k})$, with Dirac nodes at $(0, 0, \pm\pi/2)$. The term $(t_z'' \sin k_z)\sigma_z \otimes \tau_z$ breaks the inversion symmetry, splitting the Dirac nodes into Weyl nodes [44]. Thus, we adopt an effective model that describes the Weyl system with time-reversal symmetry. These symmetry behaviors described by this model are in good agreement with the t-$PtBi_2$ material [41, 42].

The *s*-wave pairing symmetry is prevalent in nature and is commonly observed in phonon-mediated superconductors. It has also been realized in cold-atom systems [45, 46]. Given this ubiquity, it is reasonable to assume an *s*-wave pairing symmetry in our study. The interaction term H_Δ is considered to represent an attractive interaction within the field. We assume that the interaction strength is the same for both orbitals and can be expressed as:

$$H_\Delta = -V \sum_{li} n_{li\uparrow} n_{li\downarrow}. \tag{3}$$

This attractive interaction can be decoupled into an s-wave superconducting Hamiltonian by defining the on-site mean-field pairing order parameter $\Delta_{lii} = V\langle c_{li\uparrow} c_{li\downarrow}\rangle$. Consequently, the interaction term can be rewritten as the superconducting pairing term:

$$H_{SC} = \sum_{li} \left(\Delta_{lii} c^{\dagger}_{li\uparrow} c^{\dagger}_{li\downarrow} + \text{H.c.} \right) + \frac{\sum_{li} \Delta^2_{lii}}{V}. \tag{4}$$

To investigate the surface states, we have examined the Hamiltonian under periodic boundary conditions along the y and z directions, complemented by open boundary conditions in the x direction. The Hamiltonian is then re-expressed as:

$$\begin{aligned} H_0 = & \sum_{\mathbf{k}_{yz} l i_x \sigma} \xi_{\mathbf{k}_{yz} l \sigma} c^{\dagger}_{l,i_x\sigma}\left(\mathbf{k}_{yz}\right) c_{l,i_x\sigma}\left(\mathbf{k}_{yz}\right) \\ & - \sum_{\mathbf{k}_{yz} l i_x \sigma} \left[t_1 - (-1)^l \frac{M}{2} \right] \left[c^{\dagger}_{l,i_x\sigma}\left(\mathbf{k}_{yz}\right) c_{l,i_x+1\sigma}\left(\mathbf{k}_{yz}\right) + \text{h.c.} \right] \\ & + \sum_{\mathbf{k}_{yz} i_x \sigma} \sigma t' \sin k_y \left[c^{\dagger}_{1,i_x\sigma}\left(\mathbf{k}_{yz}\right) c_{2,i_x\sigma}\left(\mathbf{k}_{yz}\right) + \text{h.c.} \right] \\ & + \sum_{\mathbf{k}_{yz} i_x \sigma} \frac{t'}{2} \left[c^{\dagger}_{1,i_x\sigma}\left(\mathbf{k}_{yz}\right) c_{2,i_x+1,\sigma}\left(\mathbf{k}_{yz}\right) \right. \\ & \left. - c^{\dagger}_{1,i_x+1,\sigma}\left(\mathbf{k}_{yz}\right) c_{2,i_x,\sigma}\left(\mathbf{k}_{yz}\right) + \text{h.c.} \right], \end{aligned} \tag{5}$$

where $\xi_{\mathbf{k}_{yz} l\sigma} = -2t_1 \cos k_y - 2t_2 \cos k_z - \mu - (-1)^l t'_z \cos k_z - (-1)^l \sigma t''_z \sin k_z - (-1)^l M(2 - \cos k_y)$. Here, σ takes $+$ for spin-up and $-$ for spin-down quasiparticles, respectively.

The superconducting pairing component is reformulated as follows:

$$H_{\text{SC}} = \sum_{\mathbf{k}_{yz} l i_x} \left[\Delta_{l i_x i_x} c^{\dagger}_{l i_x\uparrow}\left(\mathbf{k}_{yz}\right) c^{\dagger}_{l i_x\downarrow}\left(-\mathbf{k}_{yz}\right) + \text{H.c.} \right] + N_y N_z \frac{\sum_{l i_x} \Delta^2_{l i_x i_x}}{V}, \tag{6}$$

where the vector $\mathbf{k}_{yz}$ denotes a position in the two-dimensional momentum space, given by $\mathbf{k}_{yz} = (k_y, k_z)$.

The Hamiltonian can be diagonalized by solving the Bogoliubov–de Gennes (BdG) equations:

$$\sum_{l' j_x} \begin{pmatrix} H_{l i_x l' j_x\uparrow}\left(\mathbf{k}_{yz}\right) & \Delta_{l' j_x j_x} \\ \Delta^*_{l' j_x j_x} & -H^*_{l i_x l' j_x\downarrow}\left(-\mathbf{k}_{yz}\right) \end{pmatrix} \Psi^{\eta}_{l' j_x} = E_\eta \Psi^{\eta}_{l' j_x}, \tag{7}$$

with the wavefunction $\Psi^{\eta}_{l' j_x} = \left[u^{\eta}_{l' j_x\uparrow}(\mathbf{k}_{yz}), v^{\eta}_{l' j_x\downarrow}(-\mathbf{k}_{yz}) \right]^T$. Here, $H_{l i_x l' j_x\sigma}(\mathbf{k}_{yz})$ represents the normal state intra- and inter-orbital hopping term, which is obtained from equation (5).

The superconducting order parameter $\Delta_{l i_x i_x}$ is calculated self-consistently:

$$\Delta_{l i_x i_x} = \frac{V}{2 N_y N_z} \sum_{\mathbf{k}_{yz} \eta} u^{\eta}_{l i_x\uparrow}\left(\mathbf{k}_{yz}\right) v^{\eta *}_{l i_x\downarrow}\left(-\mathbf{k}_{yz}\right) \tanh\left[\frac{E_\eta\left(\mathbf{k}_{yz}\right)}{2 k_B T} \right]. \tag{8}$$

In the reduced low-dimensional system, the spectral functions depending on the reduced momentum $\mathbf{k}_{yz}$ and x are obtained as:

$$A_{l i_x\sigma}\left(\mathbf{k}_{yz}, \omega\right) = -\frac{1}{\pi} \sum_{\eta} \text{Im}\left(\frac{|u^{\eta}_{l i_x\sigma}\left(\mathbf{k}_{yz}\right)|^2}{\omega - E_\eta\left(\mathbf{k}_{yz}\right) + i\Gamma} \right). \tag{9}$$

The x-dependent LDOS is then expressed as:

$$\rho_{i_x}(\omega) = \sum_{l \mathbf{k}_{yz} \sigma} A_{l i_x\sigma}\left(\mathbf{k}_{yz}, \omega\right). \tag{10}$$

In the subsequent results, aligning with the methodology of [44], we have adopted the hopping constant t' as our energy unit, with t' normalized to 1. The remaining parameters are configured as follows: $t_1 = t_2 = 0$, $t'_z = t''_z = \frac{\sqrt{2}}{2}$, and $M = 1$. Under these conditions, the Hamiltonian (equation (2)) serves as a minimum model that describes a Weyl metal maintaining time-reversal symmetry and harboring four Weyl nodes [44]. Unless stated otherwise, the chemical potential is set at $\mu = 0.5$, and we incorporate a small value for the broadening parameter, $\Gamma = 0.005$.

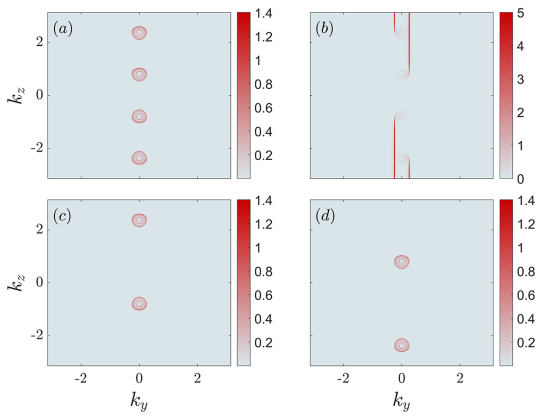

Figure 1. Intensity plots of normal-state zero-energy spectral functions with open-boundary condition along the x direction ($1 \leqslant i_x \leqslant 100$). (a) The spectral function at the system bulk with $x = 50$. (b) The spectral function in the system surface with $x = 1$. (c) The bulk spectral function for the spin-up quasiparticles. (d) The bulk spectral function for the spin-down quasiparticles.

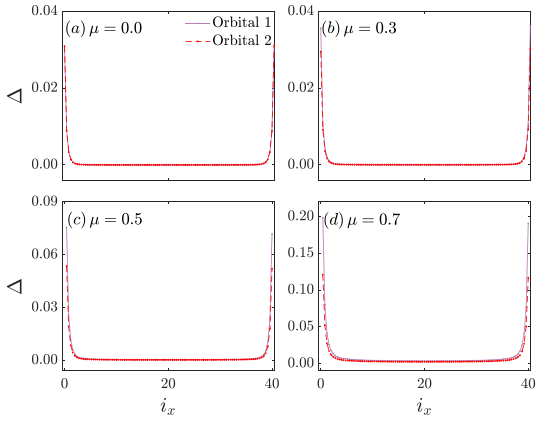

Figure 2. Numerical results of superconducting order parameters from self-consistent calculations with the pairing potential $V = 6$.

3. Results and discussion

We first present our numerical results in the normal state. Considering the open boundary condition along the x direction and the periodic boundary condition along the y and z directions, the zero-energy spectral function $A_{i_x}\left(k_y, k_z, \omega\right) = 0$ in the bulk and at the system surface are shown in figures 1(a) and (b), respectively. As observed, in the system bulk, there are four Weyl points at the momenta $\pm\mathbf{Q_1}$ and $\pm\mathbf{Q_2}$ with $\mathbf{Q_1} = (0, 0, 3\pi/4)$ and $\mathbf{Q}_2 = (0, 0, \pi/4)$. Each Weyl point is surrounded by a Fermi pocket. At the system surface, the spectra include several disconnected Fermi arcs, indicating the topological features of the system.

The intensity plots of the spectral function in the system bulk for the spin-up and spin-down quasiparticles are presented in figures 1(c) and (d), respectively. As observed, each Weyl pocket is spin-polarized; the Weyl pockets surrounding $\mathbf{Q_1}$ and $-\mathbf{Q_2}$ are contributed by the spin-up quasiparticles, while those surrounding $\mathbf{Q_2}$ and $-\mathbf{Q_1}$ are contributed by the spin-down ones. This finding is markedly different from the behavior observed in Weyl metals that possess inversion symmetry and exhibit broken time-reversal symmetry, where Fermi pocket states demonstrate spin-momentum locking. Such locking could potentially precipitate the formation of finite-momentum FFLO pairing states [14] or odd-parity pairing states [15]. The interplay and competition among the FFLO pairing state, the odd-parity BCS state, and the even-parity BCS state are of significant theoretical and experimental interest. However, based on our numerical findings in this study, we conclude that the finite-momentum pairing state and the odd-parity BCS state are not favored in our system.

Now let us study the electronic structure in the superconducting state. First, we obtain the site-dependent and orbital-dependent superconducting order parameter self-consistently. The numerical results of the order parameters with different chemical potentials are presented in figure 2. When the chemical potential is zero

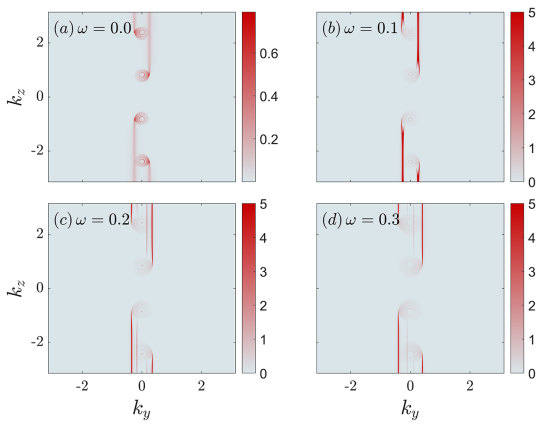

Figure 3. Intensity plots of spectral functions at the system surface in the superconducting state with open-boundary condition along the x direction ($1 \leqslant i_x \leqslant 100$).

($\mu = 0$), the superconducting order parameter is orbital-independent due to the particle-hole symmetry of the normal state Hamiltonian. As the chemical potential increases, the superconducting order parameter at the system surface increases slightly and becomes orbital-dependent, with the order parameter for orbital 1 being larger. Notably, for all parameters considered, superconductivity emerges only near the system surfaces. Away from the system surfaces, the order parameters decrease rapidly to nearly zero. Significantly, for all parameters under consideration, superconductivity is predominantly manifested near the system surfaces, while it is absent in the bulk, a phenomenon that aligns well with recent experimental findings [31, 32].

Generally, the magnitudes of the superconducting gaps are determined by the normal state density of states at the Fermi level. This observation can be understood by examining the normal state electronic structure at the Fermi energy. In the system bulk, as shown in figure 1(a), the normal state Fermi surface consists of four Fermi pockets surrounding the Weyl nodes. As previously discussed in [47], the Fermi pockets in a doped Weyl system are quite small, necessitating a relatively strong pairing interaction to achieve bulk superconductivity. In contrast, at the system's surface, as illustrated in figure 1(b), Fermi arcs are formed, and the zero-energy spectral function along these arcs exhibits significant intensity. Consequently, the density of states at the Fermi level increases substantially when moving from the bulk to the surface. Under these conditions, superconductivity tends to emerge at the system's surface.

As the chemical potential varies, these properties remain qualitatively consistent. In the supplementary material, we present the numerical results for the zero-energy LDOS and the zero-energy spectral functions at the system surface for different chemical potentials. As a result, superconductivity predominantly occurs at the system surfaces for all chemical potentials considered.

The intensity plots of spectral functions in the superconducting state at the system surface, as functions of the momentum k_y and k_z at different energies, are presented in figure 3. For all energies considered, the spectral functions include several disconnected segments. Due to the existence of the superconducting gap, the zero-energy spectral function is rather small, contributed by the tunneling of bulk states and surface states at higher energy. As the energy increases, the spectral functions are mainly contributed by the disconnected surface states.

We now present the numerical results of the LDOS spectra from the system bulk to the surface with different chemical potentials in figure 4. As observed, at the system surface, the superconducting gap and two coherence peaks are clearly visible. Note that due to the tunneling of bulk states, the LDOS spectra at the system surface are not fully gapped and residual low-energy states exist. The gap feature disappears when moving away from the system surfaces, corresponding to the disappearance of the superconducting gap in the system bulk, as presented in figure 2.

Our numerical results of the LDOS spectra for Weyl superconductors with time-reversal symmetry are significantly different from those with inversion symmetry [35]. Specifically, for Weyl superconductors with preserved inversion symmetry and broken time-reversal symmetry, no coherence peaks emerge at the system surface. Conversely, for BCS-type pairing states, the LDOS spectra exhibit a zero-energy peak at the system surface, attributable to the Fermi arc at the system surface [35] (for more details, see the supplemental material). Our results indicate that the superconducting gap feature and coherence peaks are consistent with experimental observations [31].

The difference described above can be soundly explained based on the spin texture picture. Schematic illustrations of the spin texture around the Weyl pockets are presented in figure 5. For the

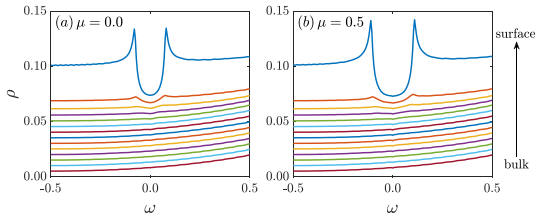

Figure 4. The LDOS spectra in the superconducting state from the system bulk to the system surface.

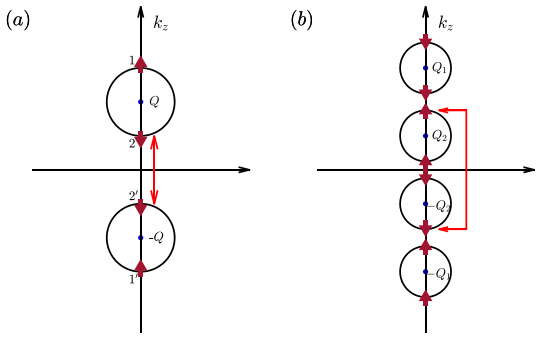

Figure 5. Schematic illustrations of the spin texture around the Weyl pockets (a) for the time-reversal-breaking system and (b) for the time-reversal preserved system.

time-reversal-breaking Weyl system, as shown in figure 5(a), the spin directions are parallel for the two quasiparticles at points 1 and 1′ or (2 and 2′). As a result, in the superconducting state with BCS-type *s*-wave pairing, the quasiparticles at points 1, 1′, 2, and 2′ cannot be paired [14]. At the system surface, disconnected Fermi arcs from 1 to 1′ and from 2 to 2′ exist, leading to the zero-energy peak [35].

In contrast, in our present work, time-reversal symmetry requires that the electronic structures for spin-up and spin-down quasiparticles at $\mathbf{k}$ and $-\mathbf{k}$, respectively, are identical. This symmetry facilitates pairing across all quasiparticles near the Fermi level in the superconducting state. Therefore, when the superconducting order parameter is nonzero, all the quasiparticles at the Fermi energy will be paired, leading to the gap feature and coherence peaks at the system surface. This spin texture also implies that the finite momentum pairing state and the odd-parity BCS state are not favored, aligning with our numerical calculations.

4. Summary

This comprehensive theoretical study presents a detailed analysis of the superconducting properties within Weyl semimetals that exhibit time-reversal symmetry. Our investigation is grounded in the framework of the BdG equations, which serve as a fundamental tool for understanding the superconducting behavior of these materials.

Our findings reveal a rich tapestry of superconducting characteristics at the surface of these Weyl semimetals, characterized by a distinct superconducting gap at the system surface in the LDOS spectra and obvious superconducting coherence peaks. This discovery is a significant departure from previous theoretical models. The presence of this gap feature is a direct consequence of the time-reversal symmetry, which plays a pivotal role in the superconducting state of these materials.

The results of our self-consistent calculations have been instrumental in bridging the gap between theoretical expectations and experimental observations. Our work aligns with recent experimental findings that have reported the observation of superconducting coherence peaks at the surface of Weyl semimetals, a feature that was previously unexplained by theoretical models. Our findings provide a theoretical basis for these observations, offering a more accurate and nuanced understanding of the superconducting properties of Weyl semimetals.

In conclusion, our study provides a comprehensive theoretical framework that elucidates the superconducting characteristics of Weyl semimetals with time-reversal symmetry. Our results highlight the critical role of time reversal symmetry in determining the superconducting behavior of these materials and

offer valuable insights that can guide future experimental and theoretical investigations in the field of topological superconductivity.

Data availability statement

All data that support the findings of this study are included within the article (and any supplementary files).

Acknowledgment

This work was supported by the NSFC (Crant No. 12074130).

ORCID iDs

W LiMing https://orcid.org/0000-0003-1348-4529
Tao Zhou https://orcid.org/0000-0003-0537-3562

References

[1] Hasan M Z, Chang G, Belopolski I, Bian G, Xu S-Y and Yin J-X 2021 *Nat. Rev. Mater.* **6** 784
[2] Lv B Q *et al* 2015 *Phys. Rev.* X **5** 031013
[3] Xu S-Y *et al* 2015 *Science* **349** 613
[4] Huang S-M *et al* 2015 *Nat. Commun.* **6** 7373
[5] Weng H, Fang C, Fang Z, Bernevig B A and Dai X 2015 *Phys. Rev.* X **5** 011029
[6] Meng T and Balents L 2012 *Phys. Rev.* B **86** 054504
[7] Das T 2013 *Phys. Rev.* B **88** 035444
[8] Chirolli L, de Juan F and Guinea F 2017 *Phys. Rev.* B **95** 201110
[9] Arrachea L and Aligia A A 2014 *Phys. Rev.* B **90** 125101
[10] Jia S, Xu S-Y and Hasan M Z 2016 *Nat. Mater.* **15** 1140
[11] Wang R, Hao L, Wang B and Ting C S 2016 *Phys. Rev.* B **93** 184511
[12] Murakami S, Hirayama M, Okugawa R and Miyake T 2017 *Sci. Adv.* **3** e1602680
[13] Chi Z *et al* 2018 *npj Quantum Mater.* **3** 28
[14] Cho G Y, Bardarson J H, Lu Y-M and Moore J E 2012 *Phys. Rev.* B **86** 214514
[15] Bednik G, Zyuzin A A and Burkov A A 2015 *Phys. Rev.* B **92** 035153
[16] Qi Y *et al* 2016 *Nat. Commun.* **7** 11038
[17] Zhang Y *et al* 2023 *Adv. Mater.* **35** 2207841
[18] Li Y *et al* 2018 *Proc. Natl Acad. Sci.* **115** 9503
[19] Guguchia Z *et al* 2017 *Nat. Commun.* **8** 1082
[20] Chan Y T, Alireza P L, Yip K Y, Niu Q, Lai K T and Goh S K 2017 *Phys. Rev.* B **96** 180504
[21] Xia J, Li D-F, Zhou J-D, Yu P, Lin J-H, Kuo J-L, Li H-B, Liu Z, Yan J-X and Shen Z-X 2017 *Small* **13** 1701887
[22] Huang C *et al* 2018 *ACS Nano* **12** 7185
[23] Tang D *et al* 2021 *Phys. Rev.* B **103** 174508
[24] Cao W *et al* 2022 *Phys. Rev.* B **105** 174502
[25] Piva M M, Kutelak L O, Borth R, Liu Y, Petrovic C, dos Reis R D and Nicklas M 2023 *Phys. Rev. Mater.* **7** L111801
[26] Zhang D, Xu Z, Le T, Chen C, Ye G, Shi F, Luo S, Shi Y and Lu X 2024 *Phys. Rev.* B **109** 144506
[27] Li Y *et al* 2017 *npj Quantum Mater.* **2** 66
[28] Bachmann M D, Nair N, Flicker F, Ilan R, Meng T, Ghimire N J, Bauer E D, Ronning F, Analytis J G and Moll P J W 2017 *Sci. Adv.* **3** e1602983
[29] Damascelli A, Hussain Z and Shen Z-X 2003 *Rev. Mod. Phys.* **75** 473
[30] Fischer O, Kugler M, Maggio-Aprile I, Berthod C and Renner C 2007 *Rev. Mod. Phys.* **79** 353
[31] Schimmel S *et al* 2024 *Nat. Commun.* **15** 9895
[32] Kuibarov A *et al* 2024 *Nature* **626** 294
[33] Nomani A and Hosur P 2023 *Phys. Rev.* B **108** 165144
[34] Shipunov G *et al* 2020 *Phys. Rev. Mater.* **4** 124202
[35] Zhou T, Gao Y and Wang Z D 2018 *Phys. Rev.* B **98** 024515
[36] Zhou T, Gao Y and Wang Z D 2016 *Phys. Rev.* B **93** 094517
[37] Shivamoggi V and Gilbert M J 2013 *Phys. Rev.* B **88** 134504
[38] Maciejko J and Nandkishore R 2014 *Phys. Rev.* B **90** 035126
[39] Khanna U, Kundu A, Pradhan S and Rao S 2014 *Phys. Rev.* B **90** 195430
[40] Okugawa R and Yokoyama T 2018 *Phys. Rev.* B **97** 060504
[41] Gao W *et al* 2018 *Nat. Commun.* **9** 3249
[42] Veyrat A *et al* 2023 *Nano Lett.* **23** 1229
[43] Hosur P, Dai X, Fang Z and Qi X-L 2014 *Phys. Rev.* B **90** 045130
[44] Hao L, Wang R, Hosur P and Ting C S 2017 *Phys. Rev.* B **96** 094530
[45] Bourdel T, Khaykovich L, Cubizolles J, Zhang J, Chevy F, Teichmann M, Tarruell L, Kokkelmans S J J M F and Salomon C 2004 *Phys. Rev. Lett.* **93** 050401
[46] Chin J K, Miller D E, Liu Y, Stan C, Setiawan W, Sanner C, Xu K and Ketterle W 2006 *Nature* **443** 961
[47] Dawson R and Aji V 2024 *Phys. Rev.* B **109** 094517